

Mechanism of Charge Transport in Hybrid Organic-Inorganic PEDOT:PSS/Silicon Heterojunctions

M. Javadi^{✉,*}, A. Mazaheri, H. Torbatiyan, and Y. Abdi[†]

Department of Physics, Nanophysics Research Laboratory, University of Tehran, Tehran 14395-547, Iran



(Received 16 April 2019; revised manuscript received 17 June 2019; published 3 September 2019)

We study the temperature and voltage dependence of current density in hybrid poly(3,4-ethylenedioxythiophene) polystyrene sulfonate (PEDOT:PSS)/Si heterojunctions. It is shown that charge transport follows distinct mechanisms at reverse and forward bias. The current is found to be injection limited at reverse bias owing to the quasi-Schottky-barrier at the organic-inorganic interface. At forward bias, the carrier transport is governed by space-charge-limited current in PEDOT:PSS. Trap-limited current at low forward bias is associated with trap states in the organic layer. The total density and the characteristic energy of localized states of PEDOT:PSS are estimated as $N_t \simeq 5.6 \times 10^{15} \text{ cm}^{-3}$ and $E_{\text{ch}} \simeq 0.107 \text{ eV}$, respectively. The commonly observed double-logarithmic character at forward bias is interpreted as the signature of transition from the Mark-Helfrich regime to the Mott-Gurney regime.

DOI: [10.1103/PhysRevApplied.12.034002](https://doi.org/10.1103/PhysRevApplied.12.034002)

I. INTRODUCTION

A hybrid organic-inorganic semiconductor heterojunction based on poly(3,4-ethylenedioxythiophene) polystyrene sulfonate (PEDOT:PSS) thin film and silicon provides a low-cost platform for silicon-based optoelectronic devices, including hybrid solar cells [1–5] and photodetectors [6,7]. This hybrid structure benefits from a straightforward and low-temperature fabrication process as well as compatibility with the mature silicon technology. Band bending at the PEDOT:PSS/Si interface gives rise to the formation of an ultrashallow depletion region at the silicon surface [8–10]. Owing to the high transparency of PEDOT:PSS, most of the incident photons are absorbed in the depleted region. This leads to the fast separation of excess photogenerated carriers with minimum internal loss in such a way that excess holes are injected into the polymer and electrons are pushed toward the bulk of silicon.

Understanding the mechanism of charge transport in the hybrid PEDOT:PSS/Si heterojunction is very important from both fundamental and technological points of view. The hybrid junction exhibits a rectifying behavior with a rectification ratio of approximately 10^3 – 10^6 . The current is thought to be controlled by the junction properties formed at the PEDOT:PSS/Si interface, which is commonly considered as a quasi-Schottky-junction [1,2,8–10] or an abrupt p^+-n junction [11–13]. While current is injection limited at reverse bias, it does not exhibit a

single-exponential rise at forward bias as is expected for thermionic emission or a one-sided abrupt p^+-n junction. Instead, there is a “kink” at around 0.4 V that results in a double-logarithmic J - V curve at forward bias [2,10,12–14]. The appearance of double-logarithmic behavior at forward bias is attributed to the bulk-transport properties of the PEDOT:PSS layer [14]. In previous studies the kink was not analyzed in detail and the origin of the kink was not fully revealed and there is lack of sufficient knowledge of the charge-transport mechanism in the organic layer.

Here we explore charge-transport properties in the hybrid PEDOT:PSS/Si heterojunction through the temperature dependence of the current-voltage characteristics. Diverse analyses based on thermionic emission (TE) and space-charge-limited-current (SCLC) theories are presented to interpret the dependence of current density on the external field and system temperature. Our findings show that while TE is adequate to interpret the carrier transport at reverse voltages, it is not the determining mechanism at forward bias. Instead, charge transport at forward bias is governed by SCLC in the organic PEDOT:PSS layer. At low and moderate forward bias, the charge transport is determined by trap-limited current and at higher voltages the current approaches the Mott-Gurney square law. Various SCLC regimes at forward bias are discussed.

II. EXPERIMENTAL SECTION

The samples are prepared in a manner similar to that we reported elsewhere [7]. University silicon wafer with 300 nm SiO_2 ($\langle 100 \rangle$, n -doped, $\rho = 1 - 10 \text{ } \Omega \text{ cm}$) and PEDOT:PSS solution (OSSILA, PH 1000) are used to

*m_javadi_b@ut.ac.ir

†y.abdi@ut.ac.ir

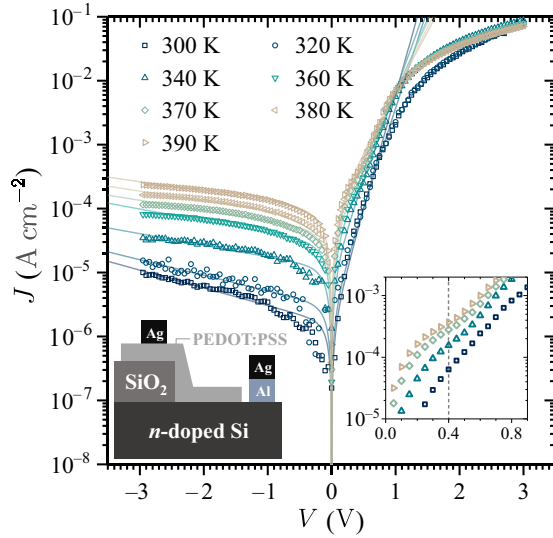


FIG. 1. Current density versus bias voltage at various temperatures. Symbols and lines represent experimental data and the corresponding fits based on Eq. (1), respectively. The inset plot shows the J - V curves in the vicinity of the kink at forward bias. A sketch of the device configuration is shown in the left inset.

prepare the samples. The conductivity of PEDOT:PSS is measured through the dependence of the conductance on the thickness of the layer and is estimated to be $0.48 \pm 0.04 \text{ S cm}^{-1}$, in agreement with the values reported for pristine PEDOT:PSS [15]. The oxide layer on silicon is removed with buffered HF solution. Aqueous PEDOT:PSS solution is spin-coated onto silicon (2000 revolutions/min, 30 s) and heated at 130°C for 10 min. The average thickness of the organic layer L is approximately 190 nm and the effective contact area at the organic-inorganic interface A_{eff} is 0.036 cm^2 . Electrical contacts are prepared by thermal evaporation of Al (50 nm)/Ag (50 nm) on silicon and thermal evaporation of 30-nm Ag on PEDOT:PSS at a base pressure of 10^{-5} Torr. The fabricated Ag/PEDOT:PSS/Si/Al/Ag structure (see the inset in Fig. 1) is chosen to be similar to the structure commonly used in hybrid solar cells. All measurements are performed in darkness and ambient conditions.

III. RESULTS AND DISCUSSION

The current-voltage characteristic of the hybrid PEDOT:PSS/Si heterojunction at various temperatures is presented in Fig. 1. As a consequence of temperature increase from 300 to 390 K, the rectification ratio (at $|V| = 3 \text{ V}$) reduces by more than 1 order of magnitude from approximately 8×10^3 to approximately 3×10^2 . The deviation from single-exponential behavior appears as a kink at $V \approx 0.4 \text{ V}$ (see the inset in Fig. 1) in harmony with previous observations [2,10,12–14].

The lowest unoccupied molecular orbital and the highest occupied molecular orbital of PEDOT:PSS are

approximately 3.4 and 5 eV below the vacuum level. From the conduction (4.05 eV) and valence (5.2 eV) bands of silicon, the band gaps of the isolated PEDOT:PSS and silicon partially overlap. Hence, the PEDOT:PSS/Si interface is categorized as a type-II (staggered) p - n heterojunction. As a result of Fermi-level alignment, a built-in potential between 0.6 and 0.9 V is developed at the interface [2,11,12]. Because of the different band gaps of PEDOT:PSS and silicon, there are discontinuities in the conduction and valence bands. In the valence band, the discontinuity comes out as a notch leading to a quasi-Schottky-barrier for hole injection from n -type silicon into the p -type PEDOT:PSS at reverse bias (Fig. 2). This discontinuity in the valence band is responsible for the inversion layer at the PEDOT:PSS/Si interface [11,12]. In the framework of thermionic emission across a Schottky barrier, the current density is related to the bias voltage (V) and ideality factor (n) as

$$J = J_0 \left[\exp \left(\frac{qV}{nk_B T} \right) - 1 \right], \quad (1)$$

where J_0 is the reverse saturation current density

$$J_0 = A^* T^2 \exp \left(-\frac{\varphi_{\text{SBH}}}{k_B T} \right), \quad (2)$$

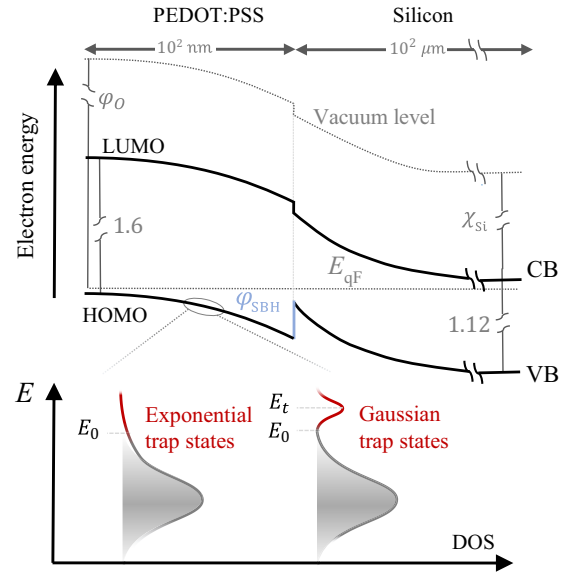


FIG. 2. Energy band diagram at the hybrid PEDOT:PSS/Si interface as a type-II (staggered) p - n heterojunction. The diagram is not to the correct scale to make band alignment clear at the interface. The density of localized states (DOS) in the exponential and Gaussian distributions is given by $D(E) = N_t/E_{\text{ch}} \exp[-(E - E_0)/E_{\text{ch}}]$ and $D(E) = N_t/\sqrt{(2\pi\sigma_t)} \exp[-(E - E_0 + E_t)^2/2\sigma_t^2]$, respectively. E_0 is the edge of the highest occupied molecular orbital (HOMO) and E_t denotes the distribution depth. CB, conduction band; LUMO, lowest unoccupied molecular orbital; VB, valence band.

where $A^* = 4\pi em^* k_B^2 / h^3$ is the Richardson constant, which for n -doped silicon is around $120 \text{ A cm}^{-2} \text{ K}^{-2}$ and φ_{SBH} is the quasi-Schottky-barrier height at the PEDOT:PSS/Si interface (Fig. 2).

Regarding to Eq. (2), the quasi-Schottky-barrier height (SBH) and effective Richardson constant can be determined from the slope and intercept of $\ln(J_0 T^{-2})$ versus $\beta = 1/k_B T$ at reverse bias. Figure 3(a) shows the Richardson plot at various reverse voltages. The curves are linear for $T \geq 320 \text{ K}$, indicating that the charge transport across the hybrid heterojunction is dominated by TE at temperatures higher than 320 K. At lower temperatures, the current flow is governed by carriers tunneling across the barrier. The extracted Schottky barrier height is presented in Fig. 3(b) as a function of reverse-bias voltage. The SBH reduces with bias voltage due to the image-force lowering, which is reflected in the bias-driven increase of the reverse saturation current (see Fig. 1). In principle, the image-force lowering of the SBH is given by $\Delta\varphi_{\text{SBH}} = \sqrt{qF/4\pi\epsilon_0\epsilon_r}$, where F is the strength of the external field at the interface [16]. In practice, the bias dependence of φ_{SBH} is commonly linearized as [17,18],

$$\varphi_{\text{SBH}} = \varphi_{\text{SBH}}^0 + q\gamma V \quad (3)$$

where φ_{SBH}^0 is the zero-bias SBH and γ is a dimensionless positive coefficient. With Eq. (3), the zero-bias SBH is

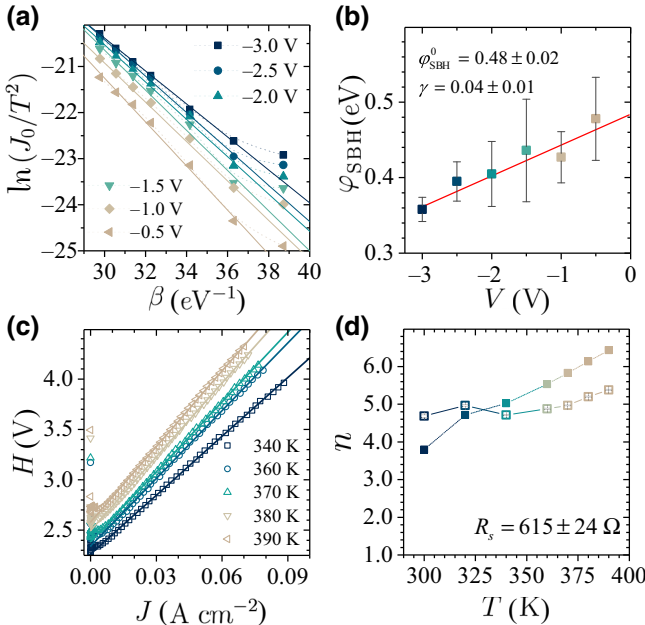


FIG. 3. Current-density analysis based on TE. (a) Richardson curves at various reverse-bias voltages. (b) The dependence of SBH on the bias voltage. The red line is the fitted curve [Eq. (3)]. (c) Forward-bias fittings of H versus current density at various temperatures [Eq. (5)]. (d) Ideality factor versus temperature. Empty and filled symbols represent data extracted from H - J curves and $n = q\beta dV/d\ln J$, respectively.

obtained as $0.48 \pm 0.04 \text{ eV}$, in agreement with the values reported for pristine PEDOT:PSS/ n -Si [14,19]. Assuming the Schottky-Mott limit, the barrier height for hole injection from silicon into PEDOT:PSS is given by $\varphi_{\text{SBH}}^0 = E_g - |\varphi_O - \chi_{\text{Si}}|$, where $E_g = 1.12 \text{ eV}$ and $\chi_{\text{Si}} = 4.05 \text{ eV}$ stand for the band gap and electron affinity of silicon, and φ_O denotes the work function of PEDOT:PSS (see Fig. 2). Putting the calculated SBH into this equation, we estimate the work function of PEDOT:PSS to be $4.69 \pm 0.04 \text{ eV}$.

From the curves shown in Fig. 3(a), the effective Richardson constant is calculated to be $3.84 (\pm 1.37) \times 10^{-4} \text{ A cm}^{-2} \text{ K}^{-2}$, orders of magnitude smaller than the expected value. The deviation is due to the presence of a thin (approximately 10 \AA) naturally grown oxide layer on the silicon surface. After colloidal PEDOT:PSS solution is dispersed onto silicon, the samples are baked at $T > 100^\circ \text{C}$ for a few minutes. This step in the fabrication process introduces a thin oxide layer onto the silicon surface. Taking into account the process of charge tunneling across the oxide layer, the Richardson constant is reduced as [20,21]

$$A_r^* = A^* \exp(-\alpha_T \delta_{\text{ox}} \sqrt{\varphi_{\text{tun}}}), \quad (4)$$

where $\alpha_T = \sqrt{8em^*}/\hbar \simeq 1.01 \text{ eV}^{-0.5} \text{ \AA}^{-1}$ is the dimensional tunneling constant, δ_{ox} is the average thickness of oxide layer (in angstroms), and φ_{tun} is the effective tunneling barrier height (in electronvolts). Using Eq. (4), we estimate the tunneling factor at the PEDOT:PSS/Si interface as $\delta_{\text{ox}} \sqrt{\varphi_{\text{tun}}} \simeq 11.6\text{--}14.4 \text{ eV}^{-0.5} \text{ \AA}$, implying an oxide thickness δ_{ox} of between 29 and 36 \AA [20].

At forward bias, holes are injected from PEDOT:PSS into n -Si. Within thermionic emission theory [Eq. (1)], the ideality factor and series resistance (R_s) can be extracted from the forward bias with use of the following equation [22]:

$$H(J) \equiv V - \frac{n}{\beta} \ln(J/A^* T^2) = A_{\text{eff}} R_s J + n\varphi_{\text{SBH}}^0 \quad (5)$$

Considering the zero-bias SBH extracted from Eq. (3), the series resistance and ideality factor are estimated from the slope and y -axis intercept of H versus J curves at various temperatures [Fig. 3(c)]. The series resistance is obtained as $615 \pm 24 \Omega$ and the extracted ideality factors are presented in Fig. 3(d) as a function of temperature. Unexpectedly, the ideality factor increases with temperature, which is not consistent with thermionic emission theory. The ideality factor is an indication of deviation from pure TE across the junction. As the temperature rises, it is expected that thermionic emission becomes the dominant process [as in the case of reverse bias, see Fig. 3(a)] and hence the ideality factor should approach 1 [23], while opposite behavior is observed. The same trend is obtained when $n = q\beta dV/d\ln J$ is used at forward bias [Fig. 3(d)]. The

increase in the ideality factor and the double-logarithmic behavior are clear signals that the charge transport at forward bias of the hybrid heterojunction is not governed by TE. In this regard, the ideality factor and other TE quantities such as the SBH and R_s extracted from *forward-bias* data are merely curve-fitting parameters and should not be interpreted as representative physical quantities.

As a result, when hybrid PEDOT:PSS/Si is reverse biased, the carrier transport through the junction is well described by thermionic emission theory. However, the experimental data do not follow the TE mechanism at forward bias. Indeed, high values of the ideality factor are an indication that the charge transport is governed by the bulk of organic layer rather than thermionic emission across the quasi-Schottky-junction [24,25]. In the following we analyze the current-voltage characteristics in the framework of space-charge-limited current. This model is often used to interpret charge transport in organic semiconductors [26–32], including emerging organic photovoltaic cells [33,34] as well as hole-only PEDOT:PSS devices [35,36]. Owing to the relative thinness of PEDOT:PSS, a considerable part of the organic layer may be depleted as a result of Fermi-level alignment at the PEDOT:PSS/Si interface (see Appendix A). In this regard, the organic layer acts as a space-charge medium and the current flow throughout the layer is governed by SCLC. In the framework of SCLC, the current generally scales with bias voltage through a power-law relation:

$$J \propto V^{m(V)}. \quad (6)$$

In the presence of an exponential tail of localized states with characteristic energy E_{ch} (see Fig. 2), three regimes are expected [37,38]. At low bias voltages, the current scales linearly with voltage due to the flow of equilibrium charge carriers. Using the multiple-trapping formalism, Röhr *et al.* [34] showed that the voltage and temperature dependence of current at low voltages is given by

$$J \propto (k_B T)^l V, \quad (7)$$

where $l = E_{ch}/k_B T$. At moderate voltages, the charge transport is dominated by thermal activation of trapped carriers and the current follows the Mark-Helfrich relation [39]

$$J \propto V^{1+l}. \quad (8)$$

At higher voltages, all the localized states will be filled by the injected carriers and charge transport obeys the trap-free Mott-Gurney square law [40]:

$$J \propto V^2. \quad (9)$$

Figure 4(a) shows the characteristic J - V curves on a logarithmic scale. With use of Eq. (6), the differential power

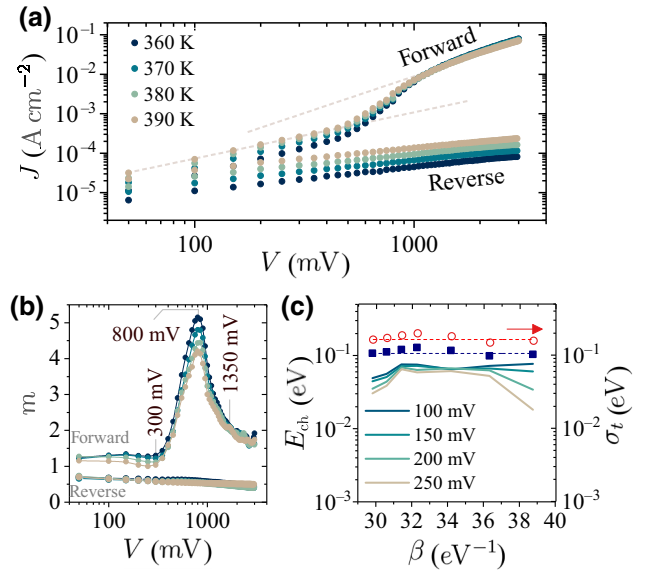


FIG. 4. Current-density analysis based on SCLC. (a) Log-log J - V curves at different temperatures. (b) Differential power versus bias voltage [Eq. (6)]. (c) Characteristic energy versus β at low forward-bias voltages extracted from Eq. (11) (lines). Squares represent the extracted E_{ch} from the Mark-Helfrich regime. The width of the distribution in the case of a Gaussian density of states is shown by empty circles [Eq. (12)].

can be calculated by

$$m(V) = \frac{\partial \log J}{\partial \log V}. \quad (10)$$

The differential power at forward and reverse bias is depicted in Fig. 4(b). At reverse bias, m is almost constant (approximately 0.5) over the scanned range independent of the system temperature. This is strong evidence of the Schottky effect, and is discussed later. At forward bias, three regimes are identified. At low voltages, m lies between 1 and 1.3 depending on the system temperature [linear regime, Eq. (7)]. The sharp rise at 300 mV signals the onset of the trap-filling process. At moderate voltages, m exhibits a maximum at 800 mV ($m \approx 4$ –5) characteristic of Mark-Helfrich regime [$m > 2$, Eq. (8)]. At higher voltages, m approaches to 2 ($m \approx 1.65$ –1.95), indicating the trap-free Mott-Gurney regime [Eq. (9)].

In the linear regime [Eq. (7)], the characteristic energy of trap states can be estimated from

$$E_{ch} = -\frac{1}{1 + \log \beta} \frac{\partial \log J}{\partial \beta}. \quad (11)$$

As shown in Fig. 4(c), E_{ch} is approximately 0.05–0.07 eV. The characteristic energy of the band tail may also be calculated from $E_{ch} = (m - 1)/\beta$ in the Mark-Helfrich regime. We use m_{\max} at 800 mV to extract E_{ch} at various temperatures; the results are depicted in Fig. 4(c).

The average value is obtained as $E_{\text{ch}} = 0.107 \pm 0.007$ eV, which is slightly higher than the estimated values from the linear regime. The discrepancy may originate from the approximations involved in Eq. (7).

The density of trap states may follow a Gaussian distribution (see Fig. 2). Just like the exponential tail, a Gaussian density of states would result in the same power relation in the Mark-Helfrich regime [Eq. (8)]. In this case, l would be related to the distribution width (σ_t) as [28,41].

$$l = \sqrt{1 + \frac{\pi}{8}(\beta\sigma_t)^2} \quad (12)$$

The calculated widths (based on m_{max}) are presented in Fig. 4(c). The average distribution width is estimated to be 0.164 ± 0.011 eV.

As discussed in the preceding paragraph, the carrier transport is trap limited at low and moderate forward bias. Trap-filled limit voltage is observed at $V_{\text{TFL}} = 1350$ mV, where charge transport enters the trap-free Mott-Gurney regime (see Appendix B). At this point, all the localized states will become filled and further increase of the applied voltage will result in the introduction of free carriers that cannot be trapped [37]. The total density of localized states (N_t) can be roughly estimated from $Q = CV_{\text{TFL}}$, where $Q = qALN_t$ is the total trapped charge and $C = \epsilon_P A/L$ is the capacitance of the organic layer. The relative permittivity of PEDOT:PSS is around 3, and hence the total density of localized states is obtained as $N_t = \epsilon_P V_{\text{TFL}}/qL^2 \simeq 5.6 \times 10^{15} \text{ cm}^{-3}$. In the Mott-Gurney regime, the current density depends solely on the mobility of carriers and is given by $J = (9/8)\epsilon\mu(V^2/L^3)$. Assuming field-independent mobility and ignoring the built-in potential at interfaces, the hole mobility of PEDOT:PSS (at $V = 3$ V) is estimated to be $\mu = 0.000268 \text{ cm}^2 \text{ V}^{-1} \text{ s}^{-1}$, in good agreement with the reported values for pristine PEDOT:PSS [36,42,43].

We now discuss $m(V) \approx 0.5$ at reverse voltages. The current saturation at reverse bias ensues from the fact that the amount of charge the quasi-Schottky-barrier supplies to PEDOT:PSS is insufficient to satisfy SCLC. Incorporating image-force lowering of the SBH into the saturation current, we can write the Schottky effect as [37]

$$J_s = J_0 \exp\left(\beta_s \sqrt{\frac{V}{L}}\right), \quad (13)$$

where J_0 is the zero-bias current density given by Eq. (2) (with φ_{SBH} replaced by φ_{SBH}^0). The external field strength is approximated by V/L and $\beta_s = \beta\sqrt{q/4\pi\epsilon_0\epsilon_r}$. The maximum value of the exponent is $\beta_s\sqrt{V/L} \approx 0.02$, which is small enough to safely approximate Eq. (13) as

$$J_s(V) \propto J_0 \beta_s \sqrt{V/L}. \quad (14)$$

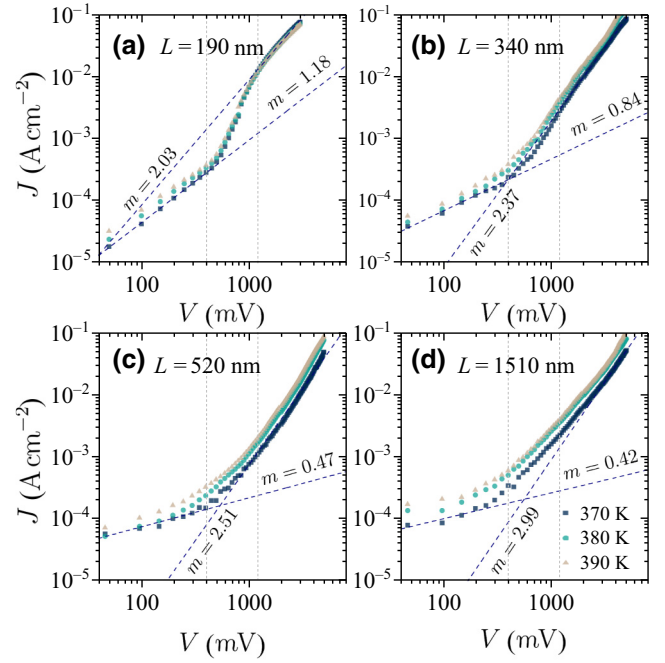


FIG. 5. The dependence of forward-bias current-voltage characteristics of the hybrid PEDOT:PSS/Si heterojunction on the thickness of the PEDOT:PSS layer.

This equation implies $\partial \log J / \partial \log V = 0.5$, which is observed at reverse bias as shown in Fig. 4(b).

Finally, we discuss the effect of the thickness of the organic layer on the charge-transport mechanism at forward bias. As mentioned previously, the appearance of SCLC in PEDOT:PSS originates from the thinness of the layer, where the width of the depletion region is comparable to the thickness of PEDOT:PSS. We investigate charge transport in various PEDOT:PSS/Si samples with different thicknesses of the PEDOT:PSS layer. Figure 5 shows logarithmic current-voltage characteristics across PEDOT:PSS/Si heterojunctions at forward bias. For the thinnest sample [Fig. 5(a)] the J - V curves obviously follow the SCLC. As the thickness of PEDOT:PSS increases, the double-logarithmic character disappears and the J - V curves tend to a single-exponential behavior in the samples with thicker PEDOT:PSS [Fig. 5(d)]. In this regard, for thin organic layers, where the width of the depletion region is comparable to the thickness of the layer, carrier transport is governed by SCLC. For thick PEDOT:PSS layers, on the other hand, the depletion width is much smaller than the thickness of the layer and it is the bulk properties (i.e., excess holes in PEDOT:PSS) that govern the carrier transport through the organic layer.

IV. CONCLUSION

In summary, carrier transport in the hybrid PEDOT:PSS/Si heterojunction is governed by distinct mechanisms at

reverse and forward voltages. At reverse bias, the current is *injection limited* via thermionic emission across the quasi-Schottky-barrier at the organic-inorganic interface. At forward bias, on the other hand, the carrier transport is essentially governed by *space-charge-limited current* in the PEDOT:PSS layer. A similar situation is observed in hybrid Methyl Red/*p*-Si [24] and Orange G/*n*-Si [25] heterojunctions as well as asymmetric spiro-OMeTAD single-carrier devices [34]. Charge transport at low and moderate forward bias is trap limited and the onset of trap filling (Mark-Helfrich regime) is at 300 mV. The transition from the Mark-Helfrich regime to the Mott-Gurney regime occurs at 1350 mV, which is the origin of the frequently observed double-logarithmic behavior at forward bias. The appearance of SCLC at forward bias strongly depends on the thickness of PEDOT:PSS. As the thickness of the organic layer increases, the double-logarithmic behavior disappears and the current density tends to increase as a single exponential. This correlation indicates that for thin PEDOT:PSS layers (which is the ideal case for optoelectronic and photovoltaic applications of hybrid PEDOT:PSS/Si heterojunctions), a considerable portion of the organic layer is depleted and the layer acts as a space-charge medium where charge transport is governed by space-charge-limited current.

ACKNOWLEDGMENTS

The authors acknowledge the Iran Science Elites Federation and the Iran National Science Foundation for partial financial support.

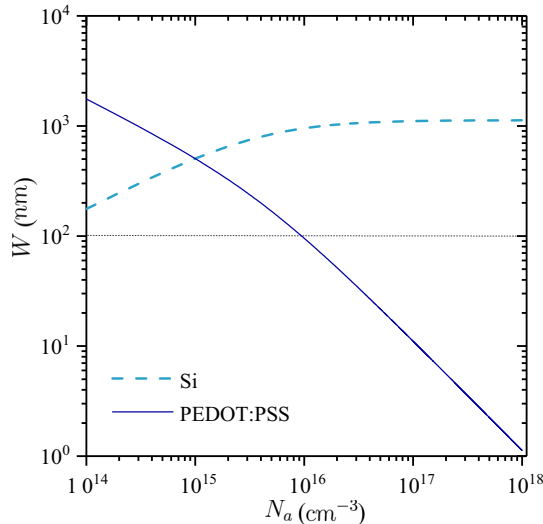


FIG. 6. Width of the depletion region in silicon and PEDOT:PSS as a function of hole concentration in the organic layer. The values of various parameters are as follows: $\psi_{bi} = 1$ eV, $N_d = 10^{15}$ cm $^{-3}$, $\epsilon_{r,Si} = 12$, $\epsilon_{r,P} = 3$.

APPENDIX A: DEPLETION APPROXIMATION

In the depletion approximation, which is often used in semiconductor heterojunctions, the depletion width on each side of the PEDOT:PSS/Si heterojunction is given by

$$W_{Si(P)} = \sqrt{\frac{2N_{a(d)}\epsilon_{Si}\epsilon_P\psi_{bi}}{qN_{a(d)}(\epsilon_{Si}N_d + \epsilon_P N_a)}}, \quad (A1)$$

where $N_{a(d)}$ denotes the concentration of carriers in the *p*-type PEDOT:PSS (*n*-type silicon) and ψ_{bi} is the contact potential. Figure 6 shows the depletion widths as a function of the carrier concentration in the organic layer. For a hole concentration of approximately 10^{16} cm $^{-3}$, the width of the depletion region in PEDOT:PSS is approximately 10^2 nm, which is the typical thickness of the organic layer. Depending on the oxidation level and the relative ratio of PEDOT to PSS, the concentration of holes in PEDOT:PSS may differ by orders of magnitude.

APPENDIX B: TRANSITION TO THE TRAP-FREE MOTT-GURNEY REGIME

Figure 7(a) presents *J-V* curves at moderate and high forward-bias voltages. At low and moderate bias, the carrier transport is governed by the multiple-trapping mechanism, which is a thermally activated process [38,44]. At these voltages, the current increases as temperature rises. It is apparent from Fig. 7(a) that the trap-filled limit voltage is around 1350 mV. This is the point where all the traps will become filled and further increase of the external field would inject *free carriers* that cannot be trapped (bandlike

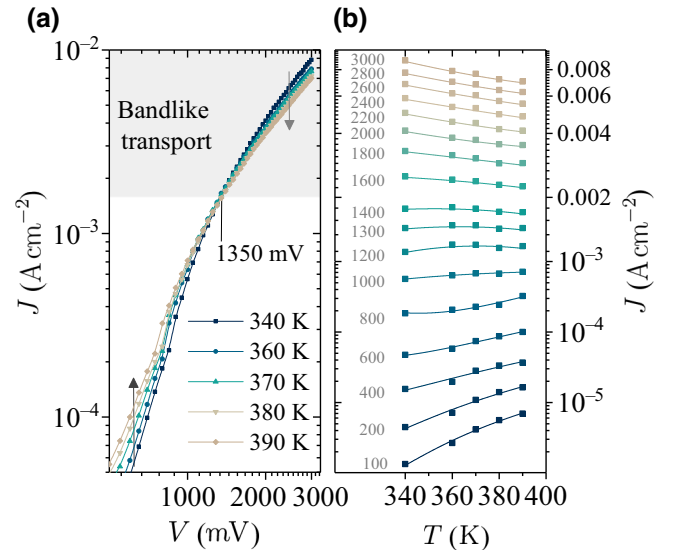


FIG. 7. (a) Current-voltage characteristics in the vicinity of the trap-filled limit voltage. (b) Temperature dependence of current density at various forward voltages.

transport). In this regard, increasing the system temperature in the Mott-Gurney regime will result in enhancement of free-carrier scattering from the lattice vibrations, and hence, the current decreases with temperature (the concentration of injected holes is much higher than that of the thermal carriers). This effect is shown in Fig. 7(b), where the current density is depicted as a function of temperature at various forward voltages. Obviously, the transition from the Mark-Helfrich regime to the Mott-Gurney regime occurs at 1350 mV.

-
- [1] S. Jeong, E. C. Garnett, S. Wang, Z. Yu, S. Fan, M. L. Brongersma, M. D. McGehee, and Y. Cui, Hybrid silicon nanocone-polymer solar cells, *Nano Lett.* **12**, 2971 (2012).
 - [2] Y. Zhang, F. Zu, S.-T. Lee, L. Liao, N. Zhao, and B. Sun, Heterojunction with organic thin layers on silicon for record efficiency hybrid solar cells, *Adv. Energy Mater.* **4**, 1300923 (2014).
 - [3] J. P. Thomas, L. Zhao, D. McGillivray, and K. T. Leung, High-efficiency hybrid solar cells by nanostructural modification in PEDOT:PSS with co-solvent addition, *J. Mater. Chem. A* **2**, 2383 (2014).
 - [4] S. Jäckle, M. Liebhaber, C. Gersmann, M. Mews, K. Jäger, S. Christiansen, and K. Lips, Potential of PEDOT:PSS as a hole selective front contact for silicon heterojunction solar cells, *Sci. Rep.* **7**, 2170 (2017).
 - [5] P. Gao, Z. Yang, J. He, J. Yu, P. Liu, J. Zhu, Z. Ge, and J. Ye, Dopant-free and carrier-selective heterocontacts for silicon solar cells: Recent advances and perspectives, *Adv. Sci.* **5**, 1700547 (2018).
 - [6] Z. Liang, P. Zeng, P. Liu, C. Zhao, W. Xie, and W. Mai, Interface engineering to boost photoresponse performance of self-powered, broad-bandwidth PEDOT:PSS/Si heterojunction photodetector, *ACS Appl. Mater. Interfaces* **8**, 19158 (2016).
 - [7] M. Javadi, M. Gholami, H. Torbatian, and Y. Abdi, Hybrid organic/inorganic position-sensitive detectors based on PEDOT:PSS/n-Si, *Appl. Phys. Lett.* **112**, 113302 (2018).
 - [8] M. J. Price, J. M. Foley, R. A. May, and S. Maldonado, Comparison of majority carrier charge transfer velocities at Si/polymer and Si/metal photovoltaic heterojunctions, *Appl. Phys. Lett.* **97**, 083503 (2010).
 - [9] Y. Zhu, T. Song, F. Zhang, S.-T. Lee, and B. Sun, Efficient organic-inorganic hybrid schottky solar cell: The role of built-in potential, *Appl. Phys. Lett.* **102**, 113504 (2013).
 - [10] X. Shen, Y. Zhu, T. Song, S.-T. Lee, and B. Sun, Hole electrical transporting properties in organic-Si schottky solar cell, *Appl. Phys. Lett.* **103**, 013504 (2013).
 - [11] A. S. Erickson, A. Zohar, and D. Cahen, n-Si-organic inversion layer interfaces: A low temperature deposition method for forming a p-n homojunction in n-Si, *Adv. Energy Mater.* **4**, 1301724 (2014).
 - [12] S. Jäckle, M. Mattiza, M. Liebhaber, G. Brönstrup, M. Rommel, K. Lips, and S. Christiansen, Junction formation and current transport mechanisms in hybrid n-Si/PEDOT:PSS solar cells, *Sci. Rep.* **5**, 13008 (2015).
 - [13] A. B. Prakoso, L. Ke, J. Wang, Z. Li, C. Jiang, and Rusli, Reverse recovery transient characteristic of PEDOT:PSS/n-Si hybrid organic-inorganic heterojunction, *Org. Electron.* **42**, 269 (2017).
 - [14] C. Pathak, J. Singh, and R. Singh, Optimizing the electrical properties of PEDOT:PSS films by co-solvents and their application in polymer photovoltaic cells, *Appl. Phys. Lett.* **111**, 102107 (2017).
 - [15] H. Shi, C. Liu, Q. Jiang, and J. Xu, Effective approaches to improve the electrical conductivity of PEDOT:PSS: A review, *Adv. Electron. Mater.* **1**, 1500017 (2015).
 - [16] S. M. Sze and K. K. Ng, *Physics of Semiconductor Devices* (John Wiley & Sons, New Jersey, USA, 2006), p. 146.
 - [17] E. H. Rhoderick, Metal-semiconductor contacts, *IEE Proc. I Solid-State Electron Devices* **129**, 1 (1982).
 - [18] A. Di Bartolomeo, Graphene schottky diodes: An experimental review of the rectifying graphene/semiconductor heterojunction, *Phys. Rep.* **606**, 1 (2016).
 - [19] C. Pathak, R. Kapoor, J. Singh, and R. Singh, Investigation of the effect of organic solvents on the electrical characteristics of PEDOT:PSS/p-Si heterojunction diodes, *Thin Solid Films* **622**, 115 (2017).
 - [20] H. Card and E. Rhoderick, Studies of tunnel MOS diodes I. interface effects in silicon schottky diodes, *J. Phys. D: Appl. Phys.* **4**, 1589 (1971).
 - [21] Y. An, A. Behnam, E. Pop, and A. Ural, Metal-semiconductor-metal photodetectors based on graphene/p-type silicon schottky junctions, *Appl. Phys. Lett.* **102**, 013110 (2013).
 - [22] S. Cheung and N. Cheung, Extraction of schottky diode parameters from forward current-voltage characteristics, *Appl. Phys. Lett.* **49**, 85 (1986).
 - [23] J. H. Werner and H. H. Güttler, Temperature dependence of schottky barrier heights on silicon, *J. Appl. Phys.* **73**, 1315 (1993).
 - [24] M. Aydın and A. Türüt, The electrical characteristics of sn/methyl-red/p-type Si/Al contacts, *Microelectron. Eng.* **84**, 2875 (2007).
 - [25] Ö. Güllü, Ş. Aydoğan, and A. Türüt, Fabrication and electrical characteristics of schottky diode based on organic material, *Microelectron. Eng.* **85**, 1647 (2008).
 - [26] V. Coropceanu, J. Cornil, D. A. da Silva Filho, Y. Olivier, R. Silbey, and J.-L. Brédas, Charge transport in organic semiconductors, *Chem. Rev.* **107**, 926 (2007).
 - [27] J. Dacuña and A. Salleo, Modeling space-charge-limited currents in organic semiconductors: Extracting trap density and mobility, *Phys. Rev. B* **84**, 195209 (2011).
 - [28] H. Nicolai, M. Mandoc, and P. Blom, Electron traps in semiconducting polymers: Exponential versus gaussian trap distribution, *Phys. Rev. B* **83**, 195204 (2011).
 - [29] X.-G. Zhang and S. T. Pantelides, Theory of Space Charge Limited Currents, *Phys. Rev. Lett.* **108**, 266602 (2012).
 - [30] P. De Bruyn, A. Van Rest, G. Wetzelaer, D. M. de Leeuw, and P. W. Blom, Diffusion-limited Current in Organic Metal-insulator-metal Diodes, *Phys. Rev. Lett.* **111**, 186801 (2013).
 - [31] N. B. Kotadiya, H. Lu, A. Mondal, Y. Ie, D. Andrienko, P. W. Blom, and G.-J. A. Wetzelaer, Universal strategy for ohmic hole injection into organic semiconductors with high ionization energies, *Nat. Mater.* **17**, 329 (2018).

- [32] N. B. Kotadiya, P. W. Blom, and G. Wetzelaer, Trap-free Space-charge-limited Hole Transport in a Fullerene Derivative, *Phys. Rev. Appl.* **11**, 024069 (2019).
- [33] D. Di Nuzzo, S. van Reenen, R. A. Janssen, M. Kemerink, and S. C. Meskers, Evidence for space-charge-limited conduction in organic photovoltaic cells at open-circuit conditions, *Phys. Rev. B* **87**, 085207 (2013).
- [34] J. A. Röhr, X. Shi, S. A. Haque, T. Kirchartz, and J. Nelson, Charge Transport in Spiro-ometad Investigated through Space-charge-limited Current Measurements, *Phys. Rev. Appl.* **9**, 044017 (2018).
- [35] M. Kemerink, S. Timpanaro, M. De Kok, E. Meulenkaamp, and F. Touwslager, Three-dimensional inhomogeneities in PEDOT:PSS films, *J. Phys. Chem. B* **108**, 18820 (2004).
- [36] S. Rutledge and A. Helmy, Carrier mobility enhancement in poly (3, 4-ethylenedioxythiophene)-poly (styrenesulfonate) having undergone rapid thermal annealing, *J. Appl. Phys.* **114**, 133708 (2013).
- [37] M. Pope and C. E. Swenberg, *Electronic Processes in Organic Crystals and Polymers* (Oxford University Press on Demand, New York, USA, 1999), p. 379.
- [38] J. A. Röhr, D. Moia, S. A. Haque, T. Kirchartz, and J. Nelson, Exploring the validity and limitations of the Mott–Gurney law for charge-carrier mobility determination of semiconducting thin-films, *J. Phys.: Condens. Matter* **30**, 105901 (2018).
- [39] P. Mark and W. Helfrich, Space-charge-limited currents in organic crystals, *J. Appl. Phys.* **33**, 205 (1962).
- [40] N. F. Mott and R. W. Gurney, *Electronic Processes in Ionic Crystals* (Oxford University Press, New York, 1940), p. 168.
- [41] S. Nevspuurek and P. Smejtek, Space-charge limited currents in insulators with the gaussian distribution of traps, *Czech. J. Phys. B* **22**, 160 (1972).
- [42] J. A. DeFranco, B. S. Schmidt, M. Lipson, and G. G. Malliaras, Photolithographic patterning of organic electronic materials, *Org. Electron.* **7**, 22 (2006).
- [43] Q. Wei, M. Mukaida, Y. Naitoh, and T. Ishida, Morphological change and mobility enhancement in PEDOT:PSS by adding co-solvents, *Adv. Mater.* **25**, 2831 (2013).
- [44] S. Baranovski, *Charge Transport in Disordered Solids with Applications in Electronics* (John Wiley & Sons, Chichester, England, 2006), Vol. 17, p. 272.